Cloud Microphysical Budget Associated with Torrential Rainfall During the Landfall of Severe Tropical Storm Bilis (2006)

WANG Donghai[1,2]* (王东海), LIU Ying[1] (刘 英), ZHU Ping[3] (朱 平), YIN Jinfang[1] (尹金方),

LI Xiaofan[4] (李小凡), and TAO Wei-Kuo[5] (陶卫国)

1 *State Key Laboratory of Severe Weather, Chinese Academy of Meteorological Sciences, Beijing* 100081*, China*

2 *Science System and Applications, Inc., Lanham, MD* 20706*, USA*

3 *Department of Earth and Environment, Florida International University, Miami, FL* 33199*, USA*

4 *NOAA/NESDIS/Center for Satellite Applications and Research, Camp Springs, MD* 20746*, USA*

5 *NASA/Goddard Space Flight Center, Greenbelt, MD* 20771*, USA*

(Received September 20, 2012; in final form December 14, 2012)

ABSTRACT

Effects of vertical wind shear, radiation, and ice clouds on cloud microphysical budget associated with torrential rainfall during landfall of severe tropical storm Bilis (2006) are investigated by using a series of analysis of two-day grid-scale sensitivity experiment data. When upper-tropospheric upward motions and lower-tropospheric downward motions occur on 15 July 2006, the removal of vertical wind shear and ice clouds increases rainfall contributions from the rainfall type (CM) associated with positive net condensation and hydrometeor loss/convergence, whereas the exclusion of cloud radiative effects and cloud-radiation interaction reduces rainfall contribution from CM. The elimination of vertical wind shear and cloud-radiation interaction increases rainfall contribution from the rainfall type (Cm) associated with positive net condensation and hydrometeor gain/divergence, but the removal of cloud radiative effects and ice clouds decreases rainfall contribution from Cm. The enhancements in rainfall contribution from the rainfall type (cM) associated with negative net condensation and hydrometeor loss/convergence are caused by the exclusion of cloud radiative effects, cloud-radiation interaction and ice clouds, whereas the reduction in rainfall contribution from cM results from the removal of vertical wind shear. When upward motions appear throughout the troposphere on 16 July, the exclusion of all these effects increases rainfall contribution from CM, but generally decreases rainfall contributions from Cm and cM.

Key words: cloud radiation effects, cloud-radiation interaction, ice clouds, cloud microphysical budget, torrential rainfall

Citation: Wang Donghai, Liu Ying, Zhu Ping, et al., 2013: Cloud microphysical budget associated with torrential rainfall during the landfall of severe tropical storm Bilis (2006). *Acta Meteor. Sinica*, **27**(2), 263–272, doi: 10.1007/s13351-013-0210-z.

1. Introduction

A precipitation system may contain rainfall cells resulting from different processes. A typical example is convective-stratiform rainfall. Convective rainfall usually shows higher rain rate than stratiform rainfall does because convective rainfall is associated with upward motions throughout the troposphere, and stratiform rainfall is related to upward motions in the mid and upper troposphere and downward motions in the lower troposphere. The dynamic effects reveal a transport of hydrometeor concentration from convective regions to raining stratiform regions, which is a major source for stratiform rainfall in many precipitation systems (e.g., Gao and Li, 2008b; Wang et al., 2009a; Shen et al., 2011). The net condensation rate is signi-

Supported by the National (Key) Basic Research and Development (973) Program of China (2012CB417204), China Meteorological Administration Special Public Welfare Research Fund (GYHY200806007, GYHY201006014, and GYHY201206039), National Natural Science Foundation of China (40875022, 40633016, and 41175064), and Basic Research Project of the State Key Laboratory of Severe Weather, Chinese Academy of Meteorological Sciences.

*Corresponding author: d.wang@hotmail.com.

ficantly larger over convective regions than over raining stratiform regions (e.g., Cui et al., 2007). The net condensation and transport of hydrometeor condensation between convective regions and raining stratiform regions are explicitly included in cloud microphysical budget. Li et al. (2011) proposed a rainfall partitioning scheme based on cloud budget, in which three rainfall types are separated. They found that all three rainfall types have significant contributions to total rainfall in the calculation of tropical rainfall during a selected period of Tropical Ocean Global Atmosphere Coupled Ocean Atmosphere Response Experiment (TOGA COARE).

Severe tropical storm Bilis (2006) caused significant economic losses and fatalities during its course from Philippines, Taiwan Region, to southeastern China in July 2006. When it landed over southern China, the torrential rainfall is associated with two very different vertical profiles of vertical velocity, i.e., strong upward motions in the mid and upper troposphere and weak downward motions in the lower troposphere on 15 July and upward motions throughout the troposphere on 16 July. The torrential rainfall case has been well simulated using a two-dimensional (2-D) cloud-resolving model experiment that is validated against available observational data (Wang et al., 2009a, 2010a), and associated sensitivity experiments have been conducted and analyzed to study the effects of vertical wind shear, radiation, and ice clouds on torrential rainfall (Wang et al., 2009b, 2010b, c). Wang et al. (2009a) validated the model simulations with available observations in terms of rain rate and reflectivity and showed a fair agreement between the simulations and observations. Wang et al. (2010a) found that dominant stratiform clouds respond to imposed weak downward motions on 15 July 2006. Convective rainfall significantly increases when imposed upward motions extend to the surface a day later. Wang et al. (2009b) revealed that the inclusion of vertical wind shear produces strong convective rainfall through the kinetic-energy conversion from imposed large-scale circulations to perturbation circulations. Wang et al. (2010b) showed that increased mean rainfall caused by the exclusion of cloud radiative effects is associated with the enhanced mean latent heat resulting from the strengthened mean radiative cooling on 15 July and that the decreased mean rainfall responds to the slowdown in the mean net condensation on 16 July. Wang et al. (2010c) found that the reduced mean rainfall caused by the removal of ice clouds is mainly associated with the suppressed mean latent heat as a result of the exclusion of deposition processes. Note that convective-stratiform rainfall separation scheme developed by Tao et al. (1993) and modified by Sui et al. (1994) has been used for rainfall analysis in Wang et al. (2009a, b, 2010b, c), in which rainfall is partitioned primarily based on the intensity of rain rate. The effects of vertical wind shear, cloud radiation, cloud-radiation interaction, and ice clouds on cloud microphysical budget in this torrential rainfall case have not been studied, although the cloud microphysical processes are directly responsible for production of precipitation.

In this study, effects of vertical wind shear, cloud radiation, cloud-radiation interaction, and ice clouds on cloud microphysical budget associated with torrential rainfall during the landfall of severe tropical storm Bilis (2006) are investigated by using a series of analysis of 2-D sensitivity cloud-resolving model experiment data. Instead of using convective-stratiform rainfall partitioning scheme, this study uses cloud microphysical budget to separate rainfall. The model and sensitivity experiments are briefly described in Section 2. The results are presented in Section 3. A summary is given in Section 4.

2. Model and sensitivity experiments

The data from 2-D sensitivity cloud-resolving model experiments conducted by Wang et al. (2009a, b, 2010b, c) are used in this study. The basic model setups are summarized in Table 1 and sensitivity experiment designs are summarized in Table 2. Other model setup details can be found in Wang et al. (2009a, b, 2010b, c), Gao and Li (2008a), and Li and Gao (2011). The experiments that exclude vertical wind shear (CNVWS), cloud radiative effects (CNCR), cloud-radiation interaction (CNCRI), and ice clouds (CNIM) are identical to the control experiment (C) except that vertical wind shear is removed

Table 1. A summary for model setups and basic experiment information

Model history	Originally developed by Soong and Ogura (1980), Soong and Tao (1980), and Tao and Simpson (1993), and modified by Li et al. (1999) and Sui et al. (1994, 1998)
Prognostic equations	Potential temperature, specific humidity, five hydrometeor species, and perturbation zonal wind and vertical velocity
Cloud microphysical schemes	Lin et al. (1983), Rutledge and Hobbs (1983, 1984), Tao et al. (1989), and Krueger et al. (1995)
Radiation schemes	Chou et al. (1991, 1998), and Chou and Suarez (1994)
Basic model parameters	Model domain of 768 km, grid mash of 1.5 km, time step of 12 s, and 33 vertical layers
Lateral boundary conditions	Cyclic
Modeling region	23°–24°N, 108°–116°E
Model integration	0800 BT 14 July–0800 BT 20 July 2006
Large-scale forcing	Vertical velocity and zonal wind (Fig. 1), and horizontal advection (figure omitted) from NCEP/GDAS (GDAS: global data assimilation system)

Table 2. Sensitivity experimental design

	Difference from control experiment (C)
CNVWS	Vertically varying large-scale zonal winds in C are replaced with mass-weighted mean large-scale zonal winds
CNCR	Total hydrometeor mixing ratio (sum of mixing ratios of five cloud species) is set to zero in the calculations of optical thickness and radiation
CNCRI	Cloud-radiation interaction is not allowed and vertical radiation profiles at each grid are imposed with same vertical radiation profiles averaged over model domain mean from C
CNIM	The ice hydrometeor mixing ratio is set to zero

by using height-independent mass-weighted mean large-scale zonal wind in CNVWS, cloud radiative effects are excluded by setting total hydrometeor mixing ratio to zero in the radiative calculations in CNCR, cloud-radiation interaction is suppressed by using C-derived mean radiative profile in CNCRI, and the ice clouds are removed by setting ice hydrometeor mixing ratio to zero in CNIM.

Mass-integrated cloud budget can be symbolically expressed by

$$P_{\mathrm{S}} = Q_{\mathrm{NC}} + Q_{\mathrm{CM}}, \tag{1}$$

where

$$P_{\mathrm{S}} = \overline{\rho} w_{\mathrm{Tr}} q_{\mathrm{r}}|_{z=0}, \tag{1a}$$

$$\begin{aligned} Q_{\mathrm{NC}} = ([P_{\mathrm{CND}}] + [P_{\mathrm{DEP}}] + [P_{\mathrm{SDEP}}] \\ +[P_{\mathrm{GDEP}}]) - ([P_{\mathrm{REVP}}] + [P_{\mathrm{MLTG}}] \\ +[P_{\mathrm{MLTS}}]), \end{aligned} \tag{1b}$$

$$Q_{\mathrm{CM}} = -\frac{\partial [q_5]}{\partial t} - \left[\frac{\partial}{\partial x}(\overline{u}^{\circ} q_5)\right] - \left[\frac{\partial}{\partial x}(u' q_5)\right], \tag{1c}$$

where P_{S} is surface rain rate at z=0; $\overline{\rho}$ is height-dependent mean air density; w_{Tr} is terminal velocity for raindrop; q_5 is sum of mixing ratios of cloud water (q_{c}), raindrop (q_{r}), cloud ice (q_{i}), snow (q_{s}), and graupel (q_{g}); u is zonal wind; Q_{NC} is the net condensation, $([P_{\mathrm{CND}}] + [P_{\mathrm{DEP}}] + [P_{\mathrm{SDEP}}] + [P_{\mathrm{GDEP}}])$ represents the cloud source term that consists of vapor condensation rate for the growth of cloud water ($[P_{\mathrm{CND}}]$), vapor deposition rates for the growth of cloud ice ($[P_{\mathrm{DEP}}]$), snow ($[P_{\mathrm{SDEP}}]$), and graupel ($[P_{\mathrm{GDEP}}]$), and $-([P_{\mathrm{REVP}}] + [P_{\mathrm{MLTG}}] + [P_{\mathrm{MLTS}}])$ denotes the cloud sink term that includes growth of vapor by evaporation of raindrop ($[P_{\mathrm{REVP}}]$), evaporation of liquid from graupel surface ($[P_{\mathrm{MLTG}}]$), and evaporation of melting snow ($[P_{\mathrm{MLTS}}]$); Q_{CM} is hydrometeor change/convergence; overbar denotes a model domain mean; prime is a perturbation from model domain mean; $[(\ )](=\int_{z_{\mathrm{b}}}^{z_{\mathrm{t}}} \overline{\rho}(\ )\mathrm{d}z)$ is mass integration, z_{t} and z_{b} are the heights of the top and bottom of the model atmosphere respectively; and superscript $^{\circ}$ is an imposed GDAS data. Following Li et al. (2011), surface rainfall can be partitioned into three types based on cloud budget Eq. (1). CM is the rainfall type associated with positive net condensation and hydrometeor loss/convergence, Cm is the rainfall type associated with positive net condensation and hydrometeor gain/divergence, and cM is the rainfall type associated with negative net condensation and hydrometeor loss/convergence. Thus, the rainfall of CM is associated with positive net condensation and hydrometeor loss/convergence, whereas the rainfalls of Cm and cM correspond to positive net condensation and hydrometeor loss/convergence, respectively.

3. Results

The contribution of each rainfall type is calculated by percentage of rainfall amount for each type over total rainfall amount (PRA) in this study. In the control experiment C, contributions to total rainfall from CM (Fig. 2b) and Cm (Fig. 3b) (∼40%) are similar, which are more than twice larger than that from cM (∼18%) (Fig. 4b) as the imposed large-scale vertical velocity shows weak descending motions in the lower troposphere and strong ascending motions in the mid and upper troposphere (see Fig. 1a) on 15 July 2006. CM and Cm have similar contributions to total rainfall in this study and Li et al. (2011), although the contributions in this study are slightly larger than those in Li et al. (2011). The result of cM shows much smaller contribution to total rainfall in rainfall case over mid-latitude continent in this study than in rainfall case over open equatorial ocean (Li et al., 2011). Fractional coverage of cM (Fig. 4a) is larger than that of CM (Fig. 3a) but is smaller than that of Cm (Fig. 4a). The positive net condensation rate of Cm (Fig. 3d) is about four times higher than that of CM (Fig. 2d), but is consumed by hydrometeor divergence for the rainfall enhancement in Cm (Fig. 3e) and only rainfall source in cM (Fig. 4d). When the ascending motions imposed in the model extend to the lower troposphere on 16 July 2006, contribution from each rainfall type is barely changed (Figs. 2c, 3c, and 4c). Fractional coverage of cM (Fig. 4a) is unchanged, whereas those of CM (Fig. 2a) and Cm (Fig. 3a) are reduced. Positive net condensation rate is increased in Cm (Fig. 3d) to intensify the advection of hydrometeor concentration from Cm to CM and cM for the rainfall intensification (Figs. 2e, 3e, and 4e).

The exclusion of vertical wind shear increases rainfall contributions from two rainfall types associated with positive net condensation (Figs. 2b and 3b) but decreases rainfall contribution from cM in both days (Fig. 4b). The increases in rainfall contribution are related to the enhanced positive net condensation in CM (Fig. 2d) and the decrease in hydrometeor gain/divergence in Cm (Fig. 3e). The reduction in rainfall contribution of cM corresponds to the decrease in hydrometeor loss/convergence (Fig. 4e). The similarity in effects of vertical wind shear on rainfall processes shown in cloud budget in the two days reveals a control of upward motions in the upward troposphere on the positive net condensation and a switch of upward motions on 16 July from downward motions on 15 July in the lower troposphere barely alters effects of vertical wind shear on three rainfall types. The removal of vertical wind shear decreases fractional coverage of cM on 15 July but increases fractional coverage of cM one day later (Fig. 4a). The increase in frac-

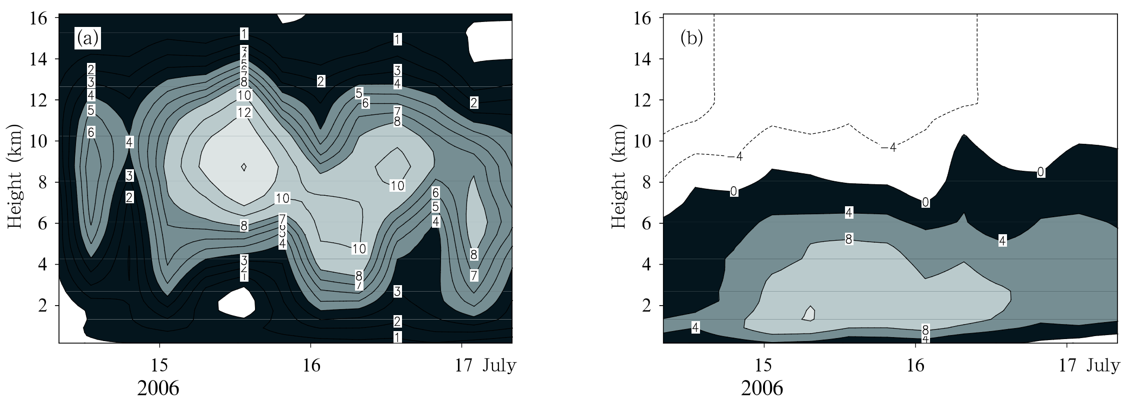

Fig. 1. Time-height distributions of (a) vertical velocity (cm s^{-1}) and (b) zonal wind (m s^{-1}) from 0800 BT 14 to 0800 BT 17 July 2006.

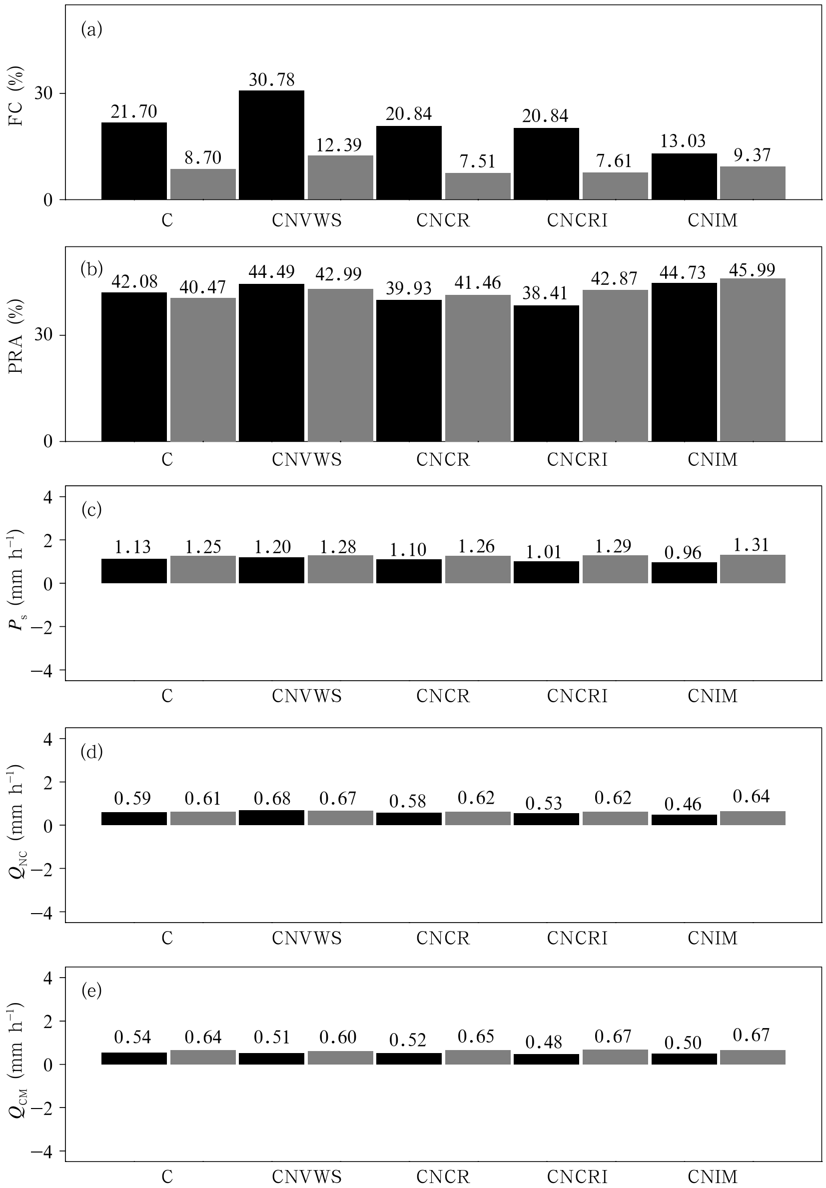

Fig. 2. (a) Fractional coverage (FC; %), (b) percentage of rain amount (PRA; %) over total rainfall amount, and model domain mean cloud budgets (mm h^{-1}) of (c) $P_{\rm S}$, (d) $Q_{\rm NC}$, and (e) $Q_{\rm CM}$ for CM daily averaged on 15 (black) and 16 (grey) July 2006.

tional coverage of cM caused by the elimination of vertical wind shear on 16 July may be associated with the reduction in perturbation kinetic energy through the removal of barotropic conversion from mean kinetic energy to perturbation kinetic energy.

The exclusion of cloud radiative effects increases positive net condensation through the enhanced latent heat caused by the increased radiative cooling in model domain mean heat and cloud budget on 15 July (Wang et al., 2010b). The increase in mean positive net condensation results from the increase in positive net condensation in Cm (Fig. 3d), which leads to the enhanced advection of hydrometeor concentration to cM (Fig. 4e) and to increase rain rate (Fig. 4c) and rainfall contribution in cM (Fig. 4b). Although the elimination of cloud radiative effects increases positive net condensation in Cm, it increases hydrometeor divergence rate of Cm (Fig. 3e). They are largely can-

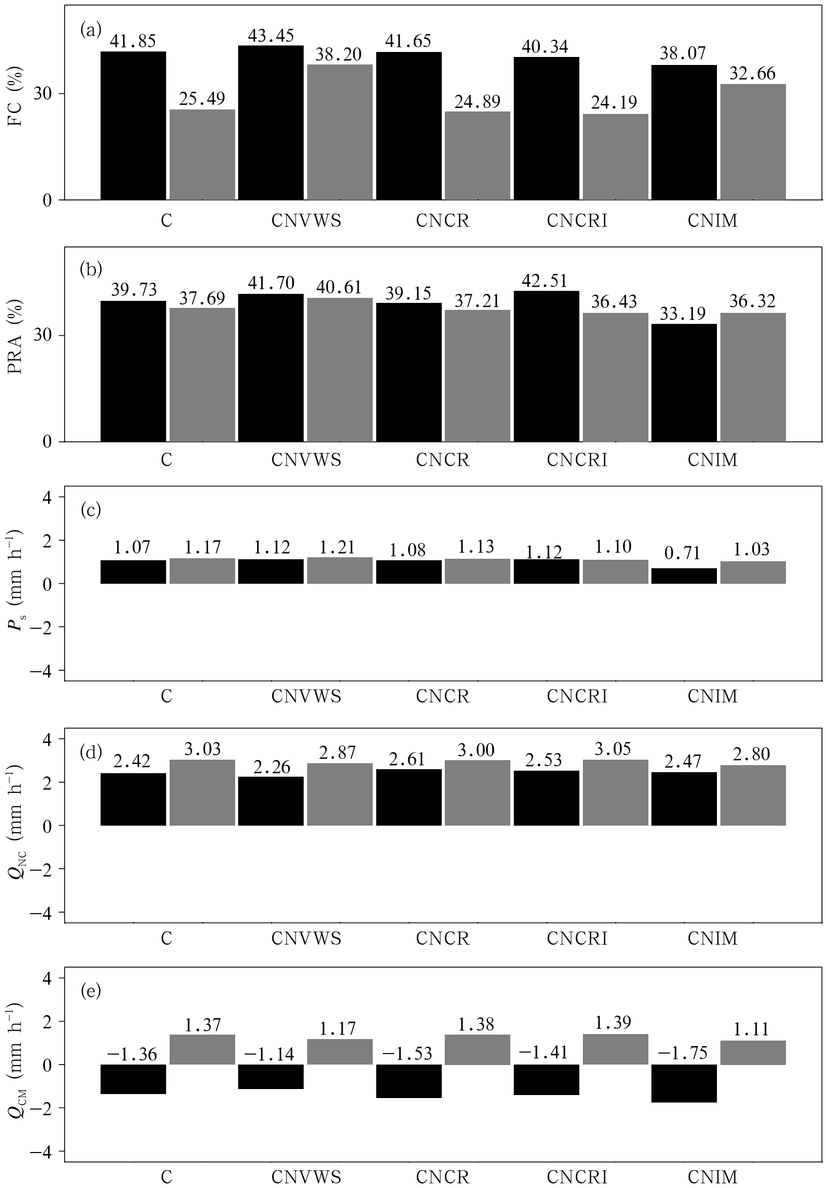

Fig. 3. As in Fig. 2, but for Cm.

celled out each other. As a result, the removal of cloud radiative effects barely changes rain rate of Cm (Fig. 3c) and slightly reduces rainfall contribution from Cm (Fig. 3b). The reduction in rainfall contribution from CM (Fig. 2b) is primarily associated with the suppressed hydrometeor loss/convergence (Fig. 2e). One day later, the exclusion of cloud radiative effects increases mean radiative cooling while it weakens mean heat divergence, which leads to the reductions of mean latent heat and associated mean net condensation (Wang et al., 2010b). The decrease in mean net condensation comes from the reduced positive net condensation in Cm (Fig. 3d) and the enhanced negative net condensation in cM (Fig. 4d). The decrease in positive net condensation causes the reduction in rainfall in Cm (Fig. 3c) while hydrometeor gain/divergence is barely changed (Fig. 3e). The enhanced negative net condensation reduces the rainfall in cM (Figs. 4c and 4d). The increase in rainfall of CM is primarily associated with the increase in positive net condensation

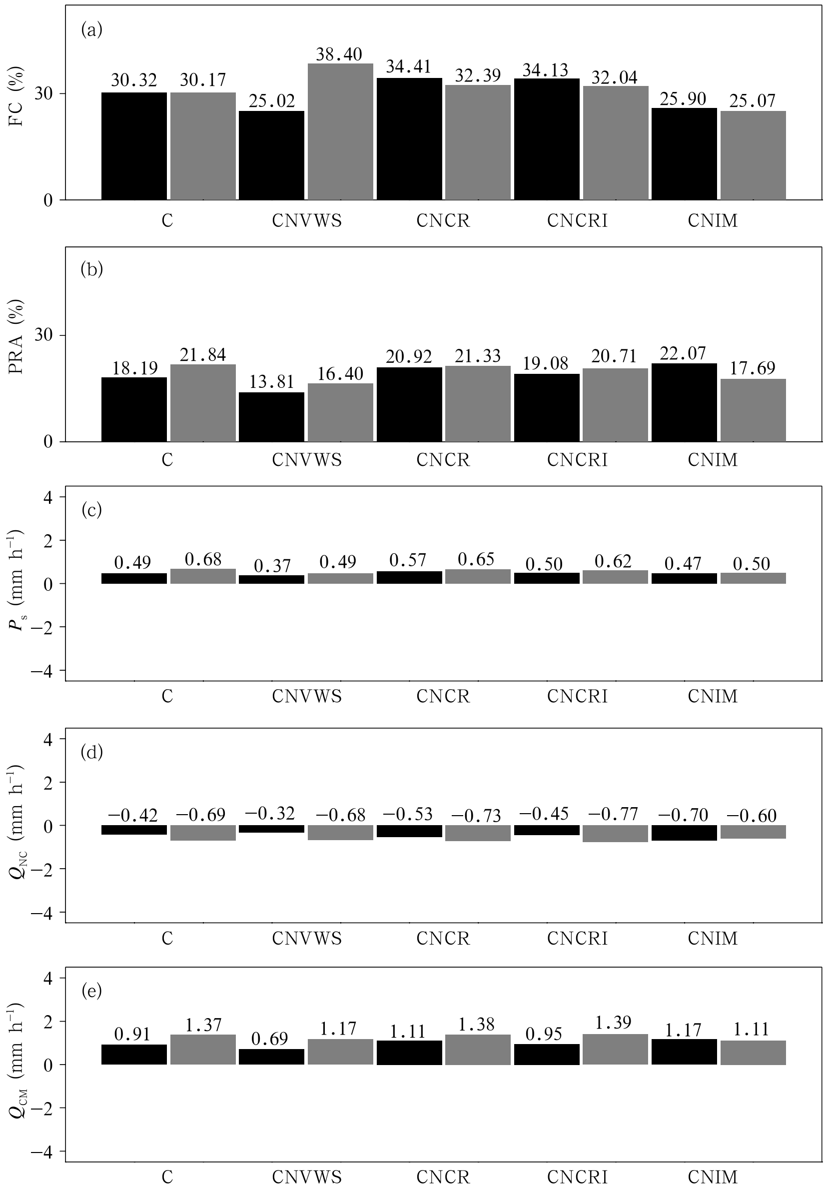

Fig. 4. As in Fig. 2, but for cM.

(Figs. 2c and 2d).

The removal of cloud-radiation interaction reduces the rain rate of CM (Fig. 2c) and its rainfall contribution (Fig. 2b) through the decreases in both positive net condensation (Fig. 2d) and hydrometeor loss/convergence (Fig. 2e), whereas it increases the rain rates of Cm and cM (Figs. 3c and 4c) and associated rainfall contributions (Figs. 3b and 4b) through the enhanced positive net condensation in Cm (Fig. 3d) and strengthened hydrometeor loss/convergence in cM (Fig. 4e) on 15 July. The exclusion of cloud-radiation interaction decreases rainfall areas of the rainfall types associated with positive net condensation (Figs. 2a and 3a), but increases rainfall area of cM (Fig. 4a). The exclusion of cloud-radiation interaction switches model domain mean hydrometeor change from loss in C to weak gain in CNCRI (Wang et al., 2010b) through the reduced hydrometeor loss/convergence of Cm (Fig. 3e). On 16 July, the elimination of cloud-radiation interaction increases the rainfall of CM (Fig. 2c) primarily through the increased hydrometeor loss/convergence (Fig. 2e) while it reduces the rainfall area of CM (Fig. 2a). The exclusion of cloud-radiation interaction reduces the rainfall and rainfall area of Cm (Figs. 3a and 3c) through the enhanced hydrometeor gain/divergence (Fig. 3e). The removal of cloud-radiation interaction decreases the rainfall of cM (Fig. 4c) through the enhanced negative net condensation (Fig. 4d) while it increases rainfall area of cM (Fig. 4a). The elimination of cloud-radiation interaction reduces model domain mean net condensation through the enhanced negative net condensation of cM (Fig. 4d) and suppresses mean hydrometeor loss through the enhanced hydrometeor gain/divergence of Cm (Wang et al., 2010b).

The exclusion of ice clouds reduces the rainfall (Figs. 2c, 3c, and 4c) and rainfall areas (Figs. 2a, 3a, and 4a) of all three rainfall types on 15 July. The reduced rainfall in CM (Fig. 2c) is primarily associated with the suppressed positive net condensation (Fig. 2d). The decrease in rainfall of Cm (Fig. 3c) is related to the enhanced hydrometeor gain/divergence (Fig. 3e). The slight reduction in rainfall of cM (Fig. 4c) corresponds to the enhanced negative net condensation (Fig. 4d), which is largely offset by the enhanced hydrometeor loss/convergence (Fig. 4e). Thus, the exclusion of ice clouds reduces model domain mean net condensation through the decrease in positive net condensation of CM (Fig. 2d) and the increase in negative net condensation of cM (Fig. 4d) and changes mean hydrometeor tendency from loss in C to gain in CNIM through the reduced hydrometeor loss/convergence of CM (Fig. 2e) and the enhanced hydrometeor gain/divergence of Cm (Fig. 3e) (Wang et al., 2010c). One day later, the removal of ice clouds reduces the rain rainfall (Figs. 3c and 4c) and rainfall areas (Figs. 3a and 4a) of Cm and cM, whereas it increases the rainfall and rainfall area of CM (Figs. 2a and 2c). The increase in rain rate of CM (Fig. 2c) is associated with the increases in positive net condensation (Fig. 2d) and hydrometeor loss/convergence (Fig. 2e) as the rainfall area in CM expands from C to CNIM (Fig. 2a). Although the rainfall area of Cm expands from C to CNIM (Fig. 3a), the decrease in rain rate of Cm (Fig. 3c) is related to the reduction in positive net condensation (Fig. 3d). The reduction in rain rate of cM (Fig. 4c) corresponds to the suppressed hydrometeor loss/convergence (Fig. 4e) as the rainfall area of cM shrinks from C to CNIM (Fig. 4a). Thus, the removal of ice clouds decreases model domain mean net condensation through the suppressed positive net condensation of Cm (Fig. 3d) and switches mean hydrometeor change from loss in C to gain in CNIM through the suppressed hydrometeor loss/convergence of cM (Fig. 4e) (Wang et al., 2010c).

4. Summary

A rainfall partitioning analysis based on cloud budget is conducted to study the effects of vertical wind shear, cloud radiation, cloud-radiation interaction, and ice clouds on torrential rainfall associated with the landfall of severe tropical storm Bilis (2006). The grid-scale data from a series of two-dimensional cloud-resolving sensitivity experiments from Wang et al. (2009a, b, 2010b, c) are used in this study. Two days of 15 and 16 July were chosen for analysis because of different vertical profiles of imposed large-scale vertical velocity: strong upward motions in the upper troposphere and weak downward motions in the lower troposphere on 15 July, and downward movement of upward motions to the mid troposphere in the morning of 16 July. The major results are drawn as follows.

(1) The rainfall type associated with positive net condensation and hydrometeor loss/convergence (CM) and the rainfall type associated with positive net condensation and hydrometeor gain/divergence (Cm) show similar contributions to total rainfall, which are larger than the contributions from the rainfall type with negative net condensation and hydrometeor loss/convergence (cM) on 15 July. The rainfall contributions from CM and Cm become smaller while that from cM becomes larger one day later.

(2) The exclusion of vertical wind shear increases rainfall contributions from CM and Cm but reduces rainfall contribution from cM on both days. This suggests that the change in rainfall contributions for all three rainfall types caused by the removal of vertical wind shear is not sensitive to vertical profile of imposed large-scale vertical velocity.

(3) The elimination of cloud radiative effects and cloud-radiation interaction decreases rainfall contribution from CM but increases rainfall contribution from cM on 15 July. The removal of cloud radiative effects and cloud-radiation interaction enhances rainfall contribution from CM but suppresses rainfall contribution from Cm and cM on 16 July. This indicates that the change in rainfall contributions from the two rainfall types associated with hydrometeor loss/convergence (Cm and cM) are sensitive to vertical profiles of imposed large-scale vertical velocity.

(4) The exclusion of ice clouds increases rainfall contribution from CM but reduce rainfall contribution from Cm on both days. The removal of ice clouds enhances rainfall contribution from cM on 15 July but suppresses rainfall contribution from cM on 16 July. This implies that change in rainfall contributions from the two rainfall types associated with positive net condensation (CM and Cm) is insensitive to vertical profiles of large-scale vertical velocity, but that from cM is sensitive to vertical profile of vertical velocity.

Acknowledgments. The authors thank two anonymous reviewers for their constructive comments.

REFERENCES

Chou, M. D., D. P. Kratz, and W. Ridgway, 1991: Infrared radiation parameterization in numerical climate models. *J. Climate*, **4**, 424–437.

——, and M. J. Suarez, 1994: An efficient thermal infrared radiation parameterization for use in general circulation model. NASA Tech. Memo. 104606, Vol. 3, 85 pp. Available from NASA/Goddard Space Flight Center, Code 913, Greenbelt, MD 20771.

——, ——, C. H. Ho, et al., 1998: Parameterizations for cloud overlapping and shortwave single scattering properties for use in general circulation and cloud ensemble models. *J. Atmos. Sci.*, **55**, 201–214.

Cui, X., Y. Zhu, and X. Li, 2007: Cloud microphysical properties in tropical convective and stratiform regions. *Meteor. Atmos. Phys.*, **98**, 1–11.

Gao, S., and X. Li, 2008a: *Cloud-Resolving Modeling of Convective Processes*. Springer, Dordrecht, 206 pp.

——, and ——, 2008b: Responses of tropical deep convective precipitation systems and their associated convective and stratiform regions to the large-scale forcing. *Quart. J. Roy. Meteor. Soc.*, **134**, 2127–2141.

Krueger, S. K., Q. Fu, K. N. Liou, et al., 1995: Improvement of an ice-phase microphysics parameterization for use in numerical simulations of tropical convection. *J. Appl. Meteor.*, **34**, 281–287.

Li, X., C.-H. Sui, K.-M. Lau, et al., 1999: Large-scale forcing and cloud-radiation interaction in the tropical deep convective regime. *J. Atmos. Sci.*, **56**, 3028–3042.

——, and S. Gao, 2011: *Precipitation Modeling and Quantitative Analysis*. Springer Dordrecht, 240 pp.

——, X. Shen, and J. Liu, 2011: A partitioning analysis of tropical rainfall based on cloud budget. *Atmos. Res.*, **102**, 444–451.

Lin, Y.-L., R. D. Farley, and H. D. Orville, 1983: Bulk parameterization of the snow field in a cloud model. *J. Climate Appl. Meteor.*, **22**, 1065–1092.

Rutledge, S. A., and P. V. Hobbs, 1983: The mesoscale and microscale structure and organization of clouds and precipitation in midlatitude cyclones. Part VIII: A model for the “seeder-feeder” process in warm-frontal rainbands. *J. Atmos. Sci.*, **40**, 1185–1206.

——, and ——, 1984: The mesoscale and microscale structure and organization of clouds and precipitation in midlatitude cyclones. Part XII: A diagnostic modeling study of precipitation development in narrow cold-frontal rainbands. *J. Atmos. Sci.*, **41**, 2949–2972.

Shen, X., Y. Wang, and X. Li, 2011: Effects of vertical wind shear and cloud radiatve processes on responses of rainfall to the large-scale forcing during pre-summer heavy rainfall over southern China. *Quart. J. Roy. Meteor. Soc.*, **137**, 236–249.

Soong, S. T., and Y. Ogura, 1980: Response of trade wind cumuli to large-scale processes. *J. Atmos. Sci.*, **37**, 2035–2050.

——, and W. K. Tao, 1980: Response of deep tropical cumulus clouds to mesoscale processes. *J. Atmos. Sci.*, **37**, 2016–2034.

Sui, C. H., K. M. Lau, W. K. Tao, et al., 1994: The tropical water and energy cycles in a cumulus ensemble model. Part I: Equilibrium climate. *J. Atmos. Sci.*, **51**, 711–728.

——, X. Li, and K. M. Lau, 1998: Radiative-convective processes in simulated diurnal variations of tropical oceanic convection. *J. Atmos. Sci.*, **55**, 2345–2359.

Tao, W. K., J. Simpson, and M. McCumber, 1989: An ice-water saturation adjustment. *Mon. Wea. Rev.*, **117**, 231–235.

—–, and —–, 1993: The Goddard cumulus ensemble model. Part I: Model description. *Terr. Atmos. Oceanic Sci.*, **4**, 35–72.

—–, —–, C. H. Sui, et al., 1993: Heating, moisture and water budgets of tropical and midlatitude squall lines: Comparisons and sensitivity to longwave radiation. *J. Atmos. Sci.*, **50**, 673–690.

Wang Donghai, Li Xiaofan, Tao Weikuo, et al., 2009a: Torrential rainfall processes associated with a landfall of severe tropical strom Bilis (2006): A two-dimensional cloud-resolving modeling study. *Atmos. Res.*, **91**, 94–104.

—–, —–, —–, et al., 2009b: Effects of vertical wind shear on convective development during a landfall of severe tropical storm Bilis (2006). *Atmos. Res.*, **94**, 270–275.

—–, —–, —–, 2010a: Responses of vertical structures in convective and stratiform regions to large-scale forcing during the landfall of severe tropical storm Bilis (2006). *Adv. Atmos. Sci.*, **27**, 33–46.

—–, —–, —–, 2010b: Cloud radiative effects on responses of rainfall to large-scale forcing during a landfall of severe tropical storm Bilis (2006). *Atmos. Res.*, **98**, 512–525.

—–, —–, —–, 2010c: Torrential rainfall responses to radiative and microphysical processes of ice clouds during a landfall of severe tropical storm Bilis (2006). *Meteor. Atmos. Phys.*, **109**, 115–128.